

# Efficient Satellite-Ground Interconnection Design for Low-orbit Mega-Constellation Topology

Wenhao Liu, Jiazhi Wu, Quanwei Lin, Handong Luo, Qi Zhang, Kun Qiu, *Senior Member, IEEE*, Zhe Chen, *Member, IEEE* and Yue Gao, *Fellow, IEEE*

**Abstract**—The low-orbit mega-constellation network (LMCN) is an important part of the space-air-ground integrated network system. An effective satellite-ground interconnection design can result in a stable constellation topology for LMCNs. A naïve solution is accessing the satellite with the longest remaining service time (LRST), which is widely used in previous designs. The Coordinated Satellite-Ground Interconnecting (CSGI), the state-of-the-art algorithm, coordinates the establishment of ground-satellite links (GSLs). Compared with existing solutions, it reduces latency by 19% and jitter by 70% on average. However, CSGI only supports the scenario where terminals access only one satellite, and cannot fully utilize the multi-access capabilities of terminals. Additionally, CSGI's high computational complexity poses deployment challenges. To overcome these problems, we propose the Classification-based Longest Remaining Service Time (C-LRST) algorithm. C-LRST supports the actual scenario with multi-access capabilities. It adds optional paths during routing with low computational complexity, improving end-to-end communications quality. We conduct our 1000s simulation from Brazil to Lithuania on the open-source platform Hypatia. Experiment results show that compared with CSGI, C-LRST reduces the latency and increases the throughput by approximately 60% and 40%, respectively. In addition, C-LRST's GSL switchings number is 14, whereas CSGI is 23. C-LRST has better link stability than CSGI.

**Index Terms**—Satellite Networks, Satellite-Ground Interconnection, Low-Orbit Mega-Constellation, Starlink

## I. INTRODUCTION

WITH the continuous expansion of the network scale, low-orbit mega-constellation network (LMCN), has become an important part of the future space-air-ground integrated network due to its wide coverage and all-weather characteristics [1], [2], [3], [4]. LMCN is a satellite network consisting of a series of low-orbit satellites, orbiting at an altitude between 200 and 2,000 km, which can guarantee better signal strength and lower propagation delay [5], [6], [7]. The emergence of Starlink [8], Iridium [9], and other constellations provides examples for the future construction of the space-air-ground integrated network. LMCN provides large-scale Internet access services around the world and has gradually become an important means to achieve globalization,

commercialization, and broadband of communications [10], [11], [12].

As of mid-2021, there are 12,000 satellites of Starlink already approved by the Federal Communications Commission (FCC), and the total number of Starlink satellites expected to be launched will reach 42,000 [13]. As the number of satellites increases and the constellation scale expands, the field faces many challenges, including network topology dynamics [14], radio channel coordination [15], routing algorithm design [16], and ground system design [17]. In addition to the above-mentioned research on the constellation itself, there are also some explorations of applications relying on LMCN. For example, some researchers [18], [19] study the optimization method for the training efficiency of machine learning models on satellites, thereby exploring the feasibility of using satellite networks for efficient data analysis [20], [21]. These studies focus on the application potential of satellite network systems, such as the analysis of observation images and data [22], [23], [24], [25], [26], [20], [27], [28].

For satellite-ground topology design, link switching and topology updates are frequent owing to the highly dynamic nature of LMCNs. Taking a satellite at an altitude of 550 km as an example, when the communication angle threshold is 25°, the average switching interval is only 2~3 minutes [1]. Frequent link switching leads to packet loss and degradation of network performance [29]. An end-to-end throughput measurement for Starlink shows that the throughput standard deviations for Starlink and the terrestrial network are 50.71% and 34.44% [30], respectively. This instability is likely caused by ground-satellite link (GSL) switchings due to satellite movements.

Algorithms like LRST aim to increase the average service time of satellites and reduce the frequency of GSL switchings, thereby achieving a more stable network topology and enhanced performance. Especially, the Coordinated Satellite-Ground Interconnecting (CSGI) algorithm performs optimization from a global perspective, minimizing the maximum transmission latency while maintaining stable routing and high network reachability. Compared with traditional methods, CSGI reduces the latency by 19% and the jitter by 70% on average [31].

Despite the advancements of CSGI algorithms, certain issues remain to be addressed. First, CSGI only supports the scenario that terminals can only access a visible satellite, while it cannot fully utilize the multi-access capabilities of the terminals. However, in actual scenarios, ground stations like those used by Starlink have eight antennas [32], which

This work was supported by the National Natural Science Foundation of China under Grant 62341105. (*Corresponding author: Kun Qiu.*) Wenhao Liu, Jiazhi Wu, Quanwei Lin, Handong Luo, Qi Zhang, Kun Qiu, Zhe Chen and Yue Gao are with the School of Computer Science, Fudan University, Shanghai 200438, China, and also with the Institute of Space Internet, Fudan University, Shanghai 200438, China (e-mail: liuwh23@m.fudan.edu.cn; jzwu21@m.fudan.edu.cn; qwlin22@m.fudan.edu.cn; hd-luo23@m.fudan.edu.cn; qizhang23@m.fudan.edu.cn; qkun@fudan.edu.cn; zhechen@fudan.edu.cn; gao.yue@fudan.edu.cn).

means that multiple satellites can be connected to a ground station at the same time. Second, deploying CSGI in real-world scenarios with hundreds of ground stations presents challenges. Although this algorithm simplifies the handover process, the computational complexity is exponential when initializing the satellite connections to ground stations, which is  $O(2^n)$ .

In order to overcome the problems of existing algorithms, such as CSGI, we propose the Classification-based Longest Remaining Service Time (C-LRST) algorithm in this paper. C-LRST supports the actual scenario of multi-access capabilities of the terminals, and on this basis, adds optional paths during routing with lower computational complexity. It divides visible satellites into two sets according to their flight directions, and the two access satellites come from two different sets when switching. Based on this classification strategy, the terminal can flexibly select access satellites in different flight directions when routing. Also, the core of C-LRST has a lower computational complexity, only  $O(n)$ , and is easier to deploy to scenarios with hundreds of ground stations than CSGI, whose computational complexity is  $O(2^n)$ . In our experiments, compared with current algorithms, C-LRST's network delay reduction is about 60%, the average throughput is also increased by about 40%, and the link is more stable. Briefly, this paper makes the following contributions:

- We study the problem of frequent switching of GSL in the existing satellite-ground topology design and analyse its impacts, such as route loss, frequent rerouting, large network latency fluctuations, and unstable throughput.
- By analyzing the distribution of satellites visible to ground terminals, we propose C-LRST, a satellite selection algorithm that is suitable for multi-access capabilities scenarios. In addition, C-LRST is easier to deploy due to its lower computational complexity  $O(n)$ .
- To evaluate the algorithm, we conduct experiments based on Starlink *shell 1*. The experiment results show that in our 1000s long-distance communication simulation from Brazil to Lithuania, compared with CSGI, C-LRST reduces the network latency by about 60%, and increases the average throughput by about 40%. In addition, the number of ground-satellite link switchings of C-LRST is 14, whereas CSGI is 23. C-LRST has better link stability than CSGI.
- We explore the adaptability of C-LRST in a larger-scale constellation by expanding the scale in the experiment. The results show that, compared with the basic scale, C-LRST still maintains good performance under the large scale, which proves the scalability potential of C-LRST in dense networks. In addition, through a detailed analysis of the experimental environment and the real world, we discuss the feasibility of C-LRST deployment in actual scenarios.

The rest of the paper is organized as follows. Section II introduces the background and our motivations. Section III presents the overview design, and our algorithm is explained in Section IV. Then, Section V describes our simulation experiments and analyses the results. Finally, Section VI concludes

the whole work.

## II. BACKGROUND

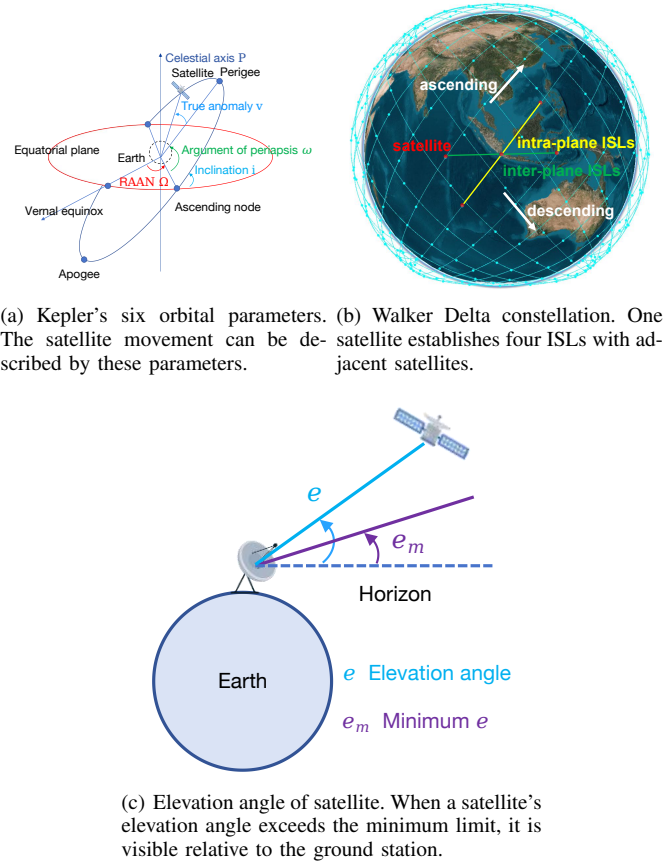


Fig. 1. Satellite and Constellation.

### A. Constellation, Links and Communications

The satellite movement can be described by Kepler's six orbital parameters, as shown in Fig. 1(a). Internationally, the two-line orbital element (TLE) [33] is generally used to describe the satellite ephemeris, which can be easily generated according to the Kepler parameters.

In this study, we focus on the Walker Delta constellation [34], as shown in Fig. 1(b). It can be described by four parameters:  $N/M/F/\alpha$ .  $N$  is the number of orbits in the constellation,  $M$  is the number of satellites in the same orbit,  $\alpha$  is the orbit inclination, and  $F$  is the phase factor used to adjust the phase difference  $\Delta f$  between two satellites in adjacent orbits with the same number in the orbit.  $\Delta f = 2\pi F/(N * M)$  and  $F$  belongs to the following range:  $\{1 - N, 2 - N, \dots, 0, 1 \dots, N - 1\}$ . A constellation usually has multiple layers of orbits. This study only considers the layer of Starlink with an altitude of 550km, called *shell 1*.

The inter-satellite link (ISL) adopts the +Grid structure [35]. Under this structure, a satellite can establish four ISLs, two connecting adjacent satellites in the same orbit, and two connecting satellites with the same number in adjacent orbits.

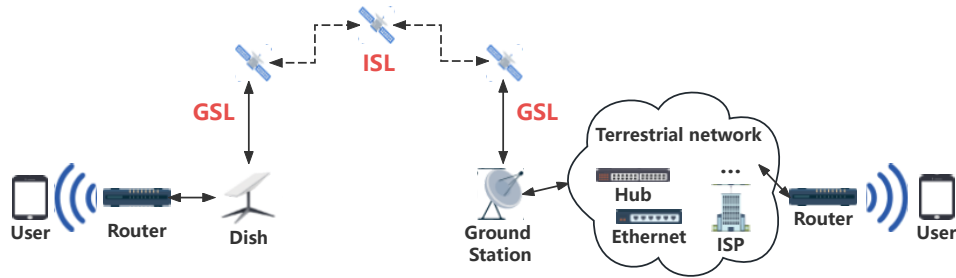


Fig. 2. ISL mode of communication between ground terminals. One ground terminal (such as a user Dish) communicates with the other (such as a ground station) through only two GSLs, with multi-hop ISLs in between.

The ground-satellite link (GSL) describes the communication between the ground station and the satellite.

In current satellite networks, there are three main methods of communication between ground terminals (such as ground stations and user Dishes).

- Transparent forwarding mode: There are no ISLs between satellites, and the communication between ground terminals is relayed through multiple GSLs.
- ISL mode: As shown in Fig. 2, one ground terminal communicates with the other through only two GSLs, with multi-hop ISLs in between.
- Hybrid mode: Ground terminals can communicate through multiple ISLs and GSLs.

Transparent forwarding mode is widely used in medium and high orbit constellations [36]. For LMCNs, the disadvantage of using Transparent forwarding mode is that it is difficult to achieve communication across continents and oceans and frequent switching of GSLs.

Starlink plans to deploy large-scale laser ISLs in the future [37], and our satellite-ground interconnection scheme will adopt the ISL mode, as shown in Fig. 2. The Hybrid mode has the shortest routing path because ground nodes are added to the network topology, but similar to the transparent forwarding mode, the network performance is greatly affected by GSL switching. We will analyse this effect through experiments in Section V to illustrate the advantages of ISL mode over Hybrid mode.

### B. Access satellite and GSL switchings

As shown in Fig. 1(c),  $e$  denotes the elevation angle of the satellite relative to the ground station. When its size exceeds the minimum elevation angle  $e_m$  of the ground station set by the system, the satellite is visible relative to the ground station [38]. When a visible satellite establishes a GSL with a ground station, it is called the access satellite of the ground station.

The number of satellites a terminal can access depends on its design. Ground stations like those used by Starlink have eight antennas [32], which means that multiple satellites can be connected to a ground station at the same time.

The altitude range of low Earth orbit (LEO) satellites is 500-1500 kilometers, and the moving speed is approximately 8 km/s [39]. For ground terminals, the satellite is visible for around 2-3 minutes [40]. This means that GSL switchings

are happening all the time, leading to network instability and frequent route changes.

### C. Classic solutions and issues

Naïve satellite-ground interconnection methods can be summarized into three categories:

- Longest remaining service time priority when switching (LRST): The ground stations connect to the satellite with the longest estimated remaining service time until it moves out of range.
- Nearest distance priority when switching (ND): The ground stations connect to the nearest satellite until it moves out of range.
- Always nearest distance priority (AND): The ground stations always connect to the nearest satellite (i.e., immediately switch to a nearer satellite when it becomes available).

According to Zhang et al. [31], in LMCN, when the ground station can access only one satellite at the same time, the performance of LRST in terms of RTT, network throughput, etc., is much better than that of ND and AND. Therefore, this paper uses the LRST algorithm as one of the baselines for comparison.

In addition, we also use the state-of-the-art algorithm, CSGI, for comparison. This algorithm is suitable for situations where the ground station can access only one satellite. When the ground station selects the access satellite, it not only considers the remaining service time but also minimizes the overall latency, thereby achieving global network optimization.

However, although the algorithm has low complexity during the handover, the computational complexity is exponential when initializing the satellite connected to the ground station, which is  $O(2^n)$ . Therefore, in a scenario with hundreds of ground stations, it cannot be deployed normally for comparison with the other algorithms. Considering this shortcoming, according to the standards of Zhang's paper, we select 15 ground stations with long distances from each other as the ground station set of CSGI algorithm. In the subsequent end-to-end path analysis experiment, the ground station pairs we use are selected from these 15 ground stations to ensure the effectiveness of the comparison experiment.

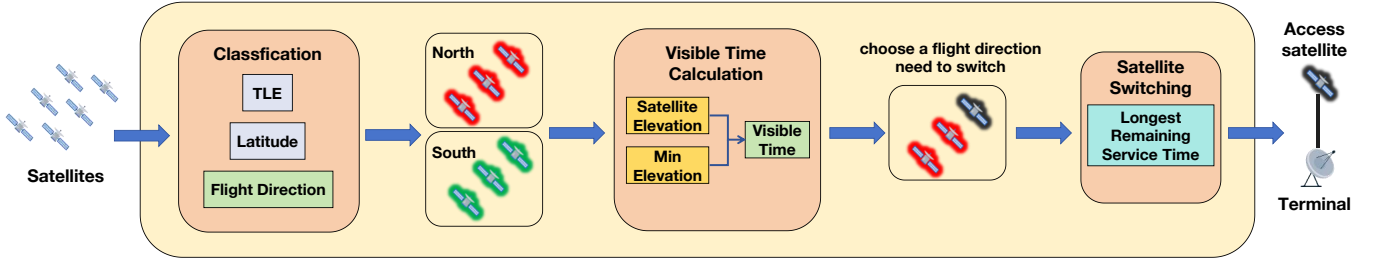


Fig. 3. Overview of C-LRST. When GSL switches, we can get a target access satellite through C-LRST. First, there are a series of visible satellites over the terminal. Through Classification operation, they are classified according to their flight directions. The output of this operation is the north set and the south set of satellites. Second, choose a flight direction that needs to be switched, such as the north. Then, calculate the visible time of all satellites in this set. Finally, select the satellite with the longest remaining service time as the target access satellite of the terminal.

### III. OVERVIEW DESIGN

The overview design of C-LRST is shown in Fig. 3. C-LRST has three main core components, *Satellite Classification* is used to classify the visible satellites of the terminal according to their flight directions. *Visible Time Calculation* is used to calculate the remaining service time of the visible satellites. Finally, the satellite with the longest remaining service time is selected as the access satellite through *Satellite Switching*. Next, we will briefly introduce its core components.

#### A. Satellite Classification

The satellites above a terminal can be divided into north and south flight directions, respectively along the orbit up and down. When selecting the access satellite, the flight direction of the satellite will affect the hop number of the ISL [41]. Based on the TLE data of the satellite, the latitudes of the current time slot and the next time slot can be calculated, and the flight direction of the satellite can be inferred, and then make classification. The access satellites of the terminal's two GSLs come from the sets of two different flight directions of its visible satellites.

#### B. Visible Time Calculation

In order to determine the satellite with the longest remaining service time in the classified set, the visible time of the satellites to the terminal needs to be calculated. Calculate the position of the satellite relative to the terminal to obtain its actual elevation  $e$ , and check whether it is greater than  $e_m$ . Since the movement of satellites is regular, the expected time for the satellite to leave the visible range of the terminal can be obtained based on the above calculation. The difference between the expected time and the current time is the visible time of the satellite.

#### C. Satellite Switching

When GSL switches, the final satellite selection is made based on the determined flight direction set and the satellite with the longest service time determined in the set. Since the terminal maintains two GSLs, when the satellite connected to one of the GSLs is switched, we only need to first determine the set of access satellites that is different from the other, and

then determine the satellite with the longest remaining service time, and finally complete the satellite selection.

### IV. ALGORITHM DESIGN

In order to support multi-access capabilities, we propose the Classification-based Longest Remaining Service Time (C-LRST) algorithm. In this section, we first present two propositions that support our algorithm. Second, we present our algorithm in detail. Finally, we introduce the execution flow of our algorithm through an example.

TABLE I  
SYMBOLS OF DEFINITIONS

Notation	Defintion
$N$	Orbit number
$M$	In-orbit satellite number
$F$	Factor
$\alpha$	Orbit inclination
$O$	The coverage area
$P$	Any point in the area
$D$	Segment length
$CL$	Chord length
$ST$	Service time
$T$	Set of time slot
$t_i$	Time slot $i$
$S$	Set of satellites
$s_i$	Satellite $i$
$G$	Set of ground stations
$g_i$	Ground station $i$
$I$	Set of ISLs
$L$	Set of GSLs
$l_i^d$	GSL of $g_i$
$C$	Set of visible satellites
$e$	Elevation angle
$e_m$	Minimum elevation angle
$d$	Flight direction of satellites

#### A. Symbols and Definitions

The key symbols used in this paper and their definitions are shown in TABLE I.  $T$  is a set of time slots in which continuous time is evenly divided according to the time slot size,  $T = \{t_0, t_1, \dots\}$ .  $S$  is the satellite set,  $S = \{s_0, s_1, \dots\}$ .  $G$  is the set of ground stations,  $G = \{g_0, g_1, \dots\}$ .  $L$  is the GSL,  $L = \{L_0, L_1, \dots\}$  and  $L_i = \{l_i^0, l_i^1\}$ .  $L_i$  record the satellites connected to  $g_i$ .  $l_i^0$  is the GSL connected to the satellites flying north and  $l_i^1$  is the GSL connected to the

satellites flying south.  $C$  is the set of visible satellites of  $g_i$ .  $e_m$  is the minimum elevation angle.  $d$  is the flight direction of satellites.  $d$  can be north or south.

### B. Theoretical Analysis

To support our algorithm, we have the following two propositions.

First, we put forward Proposition 1, analyzing the satellite switching interval through mathematical derivation. Through Proposition 1, we finally obtain the average number of link switchings within a certain time range, which is used to prove the rationality of the result of our algorithm. Second, based on Proposition 1, we further put forward Proposition 2. By analysing that satellites in the north and south flight directions have the same service time distribution, we explain the rationality of our classification operation.

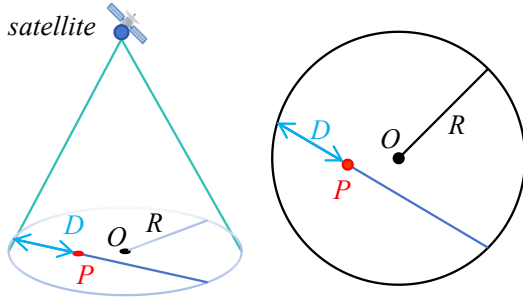


Fig. 4. Satellite service time calculation demonstration. The circle  $O$  represents the coverage area of the satellite,  $R$  is the radius of the circle,  $P$  is any point within the circle, and  $D$  represents the remaining service time along the satellite flight direction.

**Proposition 1:** The actual service time  $ST$  of the satellite is much shorter than the theoretical maximum service time  $ST_{max}$  of the satellite, and the number of switchings obtained by the C-LRST algorithm is reasonable.

**Proof 1:** We will analyse the service time and the number of switchings of the satellite with a specific beam range.

The remaining service time of a terminal's access satellite is limited by the service time of a single satellite, which will have an impact on the GSL switching interval. We will calculate this service time below.

As shown in Fig. 4, the beam coverage of the satellite on the ground can be approximately regarded as a circle  $O$ , in which the service time  $T$  to a terminal is related to the beam range, beam moving direction, and speed. Assume that the ground terminal appears with equal probability at any position within the satellite beam range. Although in actual situations, the satellite's beam will move in a fixed direction, in this analysis, considering the symmetry of the circle, we can still assume that the beam will move in any direction, so the position of the ground terminal in the beam can be expressed as any point  $P$  on any chord on the circle. The remaining service time  $ST$  of the satellite to  $P$  is approximately proportional to the length of segment  $D$  on the chord.

Therefore, our problem can be transformed into calculating the length of  $D$ .

Assume the chord length is  $CL$ . Since  $P$  is uniformly distributed on  $CL$  with equal probability, the probability density function of  $D$  is  $f(D) = \frac{1}{CL}$ . We can get the length of  $D$ .

$$\int_0^{CL} f(D)l dl = \frac{1}{CL} \cdot \frac{l^2}{2} \Big|_0^{CL} = \frac{CL}{2} \quad (1)$$

The problem is then transformed into calculating the length  $CL$  of any chord, assuming that the distance from the chord to the center of the circle is  $x$ . Since the chord is chosen arbitrarily,  $x$  is uniformly distributed within the range of  $(0, R)$ . The formula for the chord length is:

$$CL = 2\sqrt{R^2 - x^2} \quad (2)$$

in which  $x \in (0, R)$ . The average chord length is:

$$\overline{CL} = \frac{1}{R} \int_0^R 2\sqrt{R^2 - x^2} dx = \frac{\pi \cdot R}{2} \quad (3)$$

Therefore, the average length of  $D$  is:

$$\overline{D} = \frac{\overline{s}}{2} = \frac{\pi \cdot R}{4} \quad (4)$$

Due to the direct proportional relationship, if the maximum service time  $ST_{max}$  of the satellite is known, the average service time  $\overline{ST}$  of the satellite can be calculated as:

$$\overline{ST} = \frac{\pi \cdot ST_{max}}{8} \quad (5)$$

For routes with ISL, the access satellites at both ends may switch. Therefore, when the beams are continuously connected, for a certain time  $t$ , the average number of link switchings  $n$  is:

$$n = \frac{2t}{\overline{ST}} \quad (6)$$

From the above, we can conclude that our Proposition 1, actual service time is shorter than the theoretical maximum service time. For example, the  $ST_{max}$  of a satellite is estimated to be roughly 250s (satellite at 550km altitude, elevation angle 25°). After calculation, the average service time  $\overline{ST}$  of a single satellite is 98s. Within  $t = 1000s$ , the average number of link switchings  $n$  is about 20, which is similar to our subsequent experiment results.

Through the proof of Proposition 1, we can also obtain a following proposition.

**Proposition 2:** Satellites in the north and south flight directions have the same service time distribution, so the classification selection operation is reasonable.

**Proof 2:** According to the proof process of Proposition 1, satellites have an average service time  $\overline{ST}$  for terminals at any location within the beam. Therefore, a ground station with a certain position is uniformly random in the beam range of the visible satellites above. Therefore, whether the satellite is flying southward or northward, the service time of the ground station has the same service time distribution.

Although the service times may vary for specific instances, overall, due to the regular construction of the constellation, satellites in both flight directions have the same service time expectations for ground stations.

These two propositions will support our algorithm description and subsequent experiment results in Section V, proving the correctness of the results and the rationality of the classification operation.

### C. Algorithm Description

1) *C-LRST*: The idea of the longest remaining service time is to constrain the terminal to select the satellite with the longest remaining service time during GSL switching, reducing the frequency of GSL switching and thereby minimizing network performance fluctuations. Although this greedy strategy achieves its objective to a certain extent, the cost is unjustifiable. We analyse the visible satellites distribution of ground stations, as shown in Fig. 5. It is evident that there is a significant clustering phenomenon: visible satellites above the ground station fly in two directions, forming two sets. The visible satellites of ground station 60 are labeled as sets  $s_1$  and  $s_2$ , and those of ground station 46 are labeled as sets  $s_3$  and  $s_4$ .

Without a classification strategy, the satellite with the longest remaining service time chosen by ground station 60 may come from  $s_1$  or  $s_2$ , and station 46 may come from  $s_3$  or  $s_4$ . This leads to the following problem: if both ground stations ultimately select access satellites from  $s_1$  and  $s_3$ , the maximum number of ISL hops will not exceed 5. However, if the selected access satellites come from  $s_1$  and  $s_4$ , the minimum number of ISL hops will not be less than 25. The RTT ratio in both cases will be over 5x. It's not worth sacrificing such a large RTT in exchange for longer service time.

C-LRST algorithm consists of three parts: core, initialization, and handover. The function of the Core part Algorithm 1 is to obtain the longest remaining service time satellite corresponding to the flight direction at time  $t$ , when the ground terminal and satellite flight direction are specified.  $C^0$  and  $C^1$  respectively represent the set of visible satellites flying northward and southward of the ground terminal  $g_i$ . Lines 3-10 are used to calculate  $C^0$  and  $C^1$ . Lines 11-14 determine the set of candidate satellites based on the input flight direction. Lines 15-19 obtain the satellite with the longest service time in the candidate satellite set. The computational complexity of C-LRST core part is  $O(n)$ .

The function of the initialization part Algorithm 2 is to determine the two access satellites for each ground terminal at the initial moment. To obtain  $L_{G,0}$ , Algorithm 1 needs to be called twice for each ground terminal at time 0.

When a satellite, which is connected to a ground terminal through a GSL, flies out of the visible range, the GSL needs to be updated. Algorithm 3 is used to check whether any ground terminal needs to update GSL in each time slot. If an access satellite at time  $t$  flies out of the visible range at time  $t + 1$ , Algorithm 1 is called to obtain a new access satellite with the same flight direction.

2) *Proof of correctness*: We illustrate the correctness of our classification satellite selection algorithm through induction. First, for a terminal, consider that there is only one visible satellite above it, then it will be chosen as the access satellite.

---

### Algorithm 1: C-LRST

---

**Input:**  $g_i, S, d, e_m, t$

**Output:**  $c$

```

1  $C^0 = \emptyset$ 
2  $C^1 = \emptyset$ 
3 for  $s_j \in S$  do
4   calculate  $e_{i,j}$  as the elevation angle of  $s_j$  relative
   to  $g_i$  at time  $t$ 
5   if  $e_{i,j} \geq e_m$  then
6     calculate  $d_j$  as the flight direction of  $s_j$  at time
      $t$ 
7     if  $d_j$  is north then
8        $C^0 = C^0 \cup \{s_j\}$ 
9     if  $d_j$  is south then
10       $C^1 = C^1 \cup \{s_j\}$ 
11 if  $d$  is north then
12    $C = C^0$ 
13 else
14    $C = C^1$ 
15  $r = 0, c = 0$ 
16 for  $s_j \in C$  do
17   calculate  $r_{i,j,t}$  as the remaining service time of  $s_j$ 
   relative to  $g_i$  at time  $t$ 
18   if  $r_{i,j,t} \geq r$  then
19      $r = r_{i,j,t}, c = s_j$ 

```

---



---

### Algorithm 2: Initialization

---

**Input:**  $G, S, e_m$

**Output:**  $L_{G,0}$

```

1  $L_{G,0} = \emptyset$ 
2 for  $g_i \in G$  do
3    $l_{i,-1}^0 = -1, l_{i,-1}^1 = -1$ 
4   calculate  $c_0$  and  $c_1$  as the candidate satellites flying
   north or south at time 0 by algorithm 1
5    $l_{i,0}^0 = c_0, l_{i,0}^1 = c_1$ 
6    $L_{G,0} = L_{G,0} \cup \{l_{i,0}^0, l_{i,0}^1\}$ 

```

---

Second, we consider that there are two visible satellites. If the two satellites belong to the same flight direction, the one with the longest remaining service time will be selected as the access satellite. If the two satellites belong to different flight directions, they will both be chosen to establish GSLs. Third, we consider that there are multiple visible satellites, which is a general case. According to the C-LRST algorithm, visible satellites are classified, and satellites with the longest remaining service time are selected for connection. According to Proposition 2 in Section IV-B, satellites flying in the north and south flight directions have the same service time distribution. Therefore, it is reasonable to establish GSLs with satellites that have the longest remaining service time in both north and south flight directions by classifying the visible satellites.

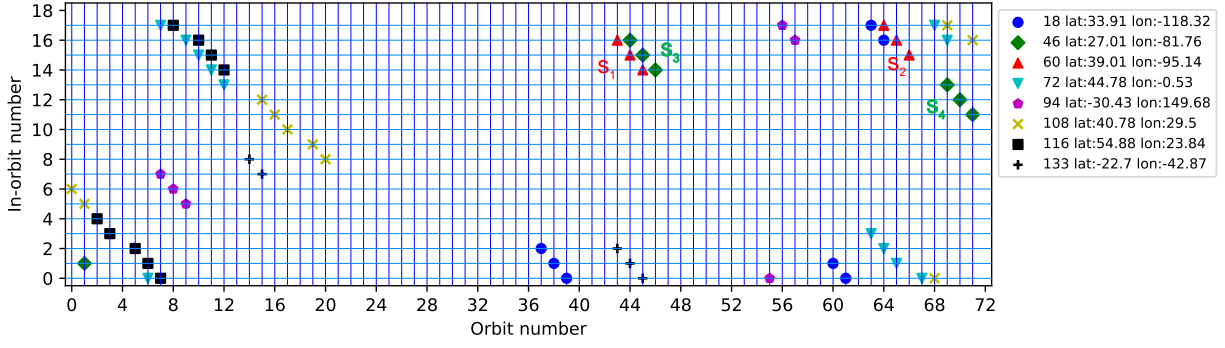


Fig. 5. Visible satellites distribution of some ground stations. Visible satellites above the ground station fly in two directions, forming two sets. For example, the visible satellites of ground station 60 are labeled as two sets  $s_1$  and  $s_2$ , and those of ground station 46 are labeled as two sets  $s_3$  and  $s_4$ .

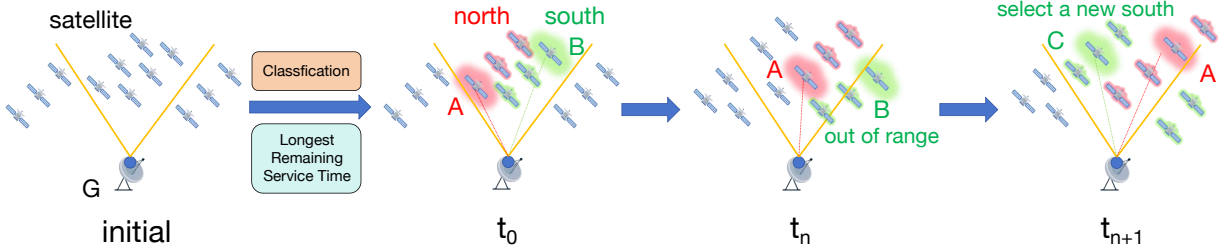


Fig. 6. Execution process of C-LRST Algorithm. This figure shows the initialization operation of ground station  $G$  and the satellite switching operation at time  $t_{n+1}$ . Initially, there are some satellites above ground station  $G$ , among which the satellites located within the elevation angle range are visible satellites of  $G$ . At time  $t_0$ , the visible satellites are classified into north and south sets according to their flight directions. The satellites with the longest service time are  $A$  and  $B$  respectively, which are selected as access satellites. Then, at time  $t_n$ ,  $A$  is still within the visible range of  $G$ , while  $B$  leaves the range. Therefore, a new satellite  $C$  will be selected from the south set at the next moment  $t_{n+1}$ .

---

### Algorithm 3: Handover

---

**Input:**  $G, S, e_m, L_{G,t}$

**Output:**  $L_{G,t+1}$

```

1  $L_{G,t+1} = \emptyset$ 
2 for  $g_i \in G$  do
3   if  $l_{i,t}^0$  is visible at time  $t+1$  then
4      $l_{i,t+1}^0 = l_{i,t}^0$ 
5   else
6     calculate  $l_{i,t+1}^0$  as the candidate satellite flying
7     north at time  $t+1$  by algorithm 1
8   if  $l_{i,t}^1$  is visible at time  $t+1$  then
9      $l_{i,t+1}^1 = l_{i,t}^1$ 
10  else
11  calculate  $l_{i,t+1}^1$  as the candidate satellite flying
12  south at time  $t+1$  by algorithm 1
13   $L_{G,t+1} = L_{G,t+1} \cup \{l_{i,t+1}^0, l_{i,t+1}^1\}$ 

```

---

#### D. Example Analysis

Next, we will describe the execution process of our algorithm through an example.

As shown in Fig. 6, there are a series of satellites above ground station  $G$ , among which the satellites located within the elevation angle range are visible satellites of  $G$ . At time  $t_0$ , the initialization operation is performed. The visible satellites are classified according to their flight directions, and the satellites

with the longest service time are selected as the two access satellites of the ground station. The satellite flying northward selected by ground station  $G$  is  $A$ , and the satellite flying southward is  $B$ . Assume that at time  $t_n$ ,  $A$  is still within the visible range of ground station  $G$ , while southward access satellite  $B$  leaves the range. We need to select a new satellite  $C$  with the longest service time from the southward set of visible satellites at the next moment  $t_{n+1}$  as the new access satellite.

## V. EXPERIMENTS

### A. Experiment Setup

We use the open-source Hypatia simulation platform developed by Kassing et al. [42], which provides a LEO satellite network simulation framework. This platform allows for the pre-computation of network states over time and implements packet-level simulations using NS-3.

In our experiments, we choose Starlink *shell 1* for study. In addition, we select 165 ground stations registered by Starlink around the world as ground nodes [43]. To ensure the adaptability of the algorithm to real satellite constellation scenarios, we conduct experiments using the actual structure of *shell 1* derived from TLE data published by Starlink [44]. TABLE II shows the detailed configurations.

Our experiments focus on the Longest Remaining Service Time algorithm that only maintains one GSL (LRST-1), the Longest Remaining Service Time algorithm that maintains

two GSLs (LRST-2), the Coordinated Satellite-Ground Interconnecting algorithm mentioned in Zhang’s paper (CSGI), and our proposed Classification-based Longest Remaining Service Time algorithm (C-LRST). The above algorithms are compared and analysed mainly based on the performance metrics of Ping, GSL switching interval, throughput, and TCP RTT.

Hypatia can construct a dynamic topology and determine the routing connectivity status between nodes within a certain simulation time by reading the configuration information of the satellites and ground stations. This is implemented by Python. Furthermore, Hypatia combines NS3 to build virtual nodes with network functions, thereby simulating constellations and ground stations. The algorithms mentioned above are different satellite-to-ground interconnection schemes that will produce different dynamic topologies and routings in the simulation. Therefore, these algorithms is implemented by modifying the topology and routing construction methods of Hypatia. We have made our implementation public online [45].

TABLE II  
STARLINK SHELL 1 PARAMETER CONFIGURATION

Parameters	Value
Orbit altitude	550 km
Orbit number ( $N$ )	72
In-orbit satellite number ( $M$ )	18
Factor ( $F$ )	45
Orbit inclination ( $\alpha$ )	$53^\circ$

### B. The impact of frequent switching

As mentioned in Section II-A, we first study the impact of frequent GSL switching in this section by comparing the performance differences between ISL mode and Hybrid mode.

Fig. 7(a) shows how the ping value changes with the distance between ground station pairs under the shortest path algorithm. This result verifies our hypothesis. During the selection of the shortest paths, for most ground station pairs, the two modes choose similar routes. For a few pairs, the paths chosen by the Hybrid mode exhibit lower ping values than the paths selected by the ISL mode. From the CDF of the average ping value shown in Fig. 7(b), we can also see that the overall distribution of ping value in ISL mode is slightly higher than that in Hybrid mode. However, as can be seen from the results of Fig. 8(a) and Fig. 8(b), shorter paths do not bring higher throughput, and the throughput in Hybrid mode is generally lower than that in ISL mode.

As shown in Fig. 9, which describes the rate of a specific pair of ground stations. Between the same ground station pair, Hybrid mode switches much more frequently than ISL mode. Multiple switchings occur within the  $65 - 100ms$  period, which significantly reduces the throughput. The decrease in throughput is due to packet loss caused by frequent path changes. However, in reality, in addition to the impact of path

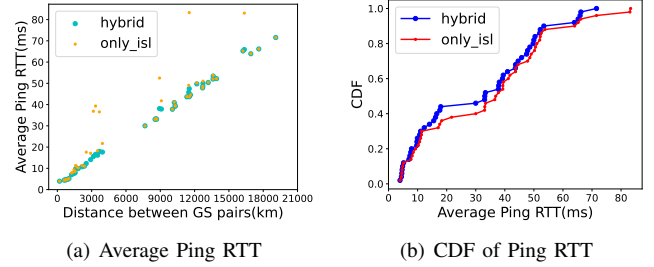


Fig. 7. Average Ping RTT over distance between ground station pairs. In most cases, Hybrid mode and ISL mode have similar ping values. Only in a few pairs, Hybrid mode has shorter paths and smaller ping values.

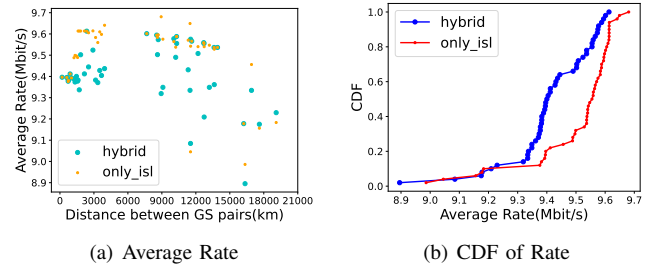


Fig. 8. Average Rate over distance between ground station pairs. In most paths, Hybrid mode exhibits poorer rate performance. This means that compared to Hybrid mode, ISL mode can achieve higher throughput.

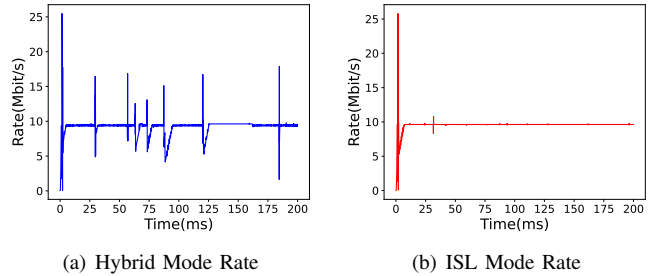


Fig. 9. Hybrid mode rate and ISL mode rate of a specific pair. This shows the reason for the different average rates above. More GSLs in Hybrid mode result in more switchings, which affect link stability and throughput.

changes on throughput and stability, GSL switching itself also has a certain overhead [29], but due to platform limitations, this aspect is not reflected in our study. Consequently, in practical applications, frequent GSL switchings result in worse performance.

### C. End-to-end path analysis

In this section, we first focus on the communication between a specific ground station pair to understand the performance of the four algorithms in detail and analyse the phenomena and causes of various indicators. Next, we study how communication between ground station nodes varies with distance to have a more comprehensive understanding of these algorithms.

Based on Hypatia, we establish end-to-end TCP links between ground stations and conduct 1000s simulation experiments. In our experiment, the NS3 time granularity is  $1ms$ , the route update interval is  $100ms$ , and the link transmission rate is set to  $10Mbit/s$ . We use TCP Hybla as the congestion



TABLE III  
LIST OF SIMULATION EXPERIMENT PARAMETERS

Parameters	Value
Simulation time	1000 s
Simulation time granularity	1 ns
Route update interval	100 ms
Transmission rate of ISL and GSL	10 Mbit/s
TCP congestion control algorithm	TCP Hybla

control algorithm. This algorithm is mainly used to solve the problem of low TCP throughput in long link scenarios, so it is often used in TCP applications of satellite networks [46]. The simulation experiment parameters are shown in TABLE III.

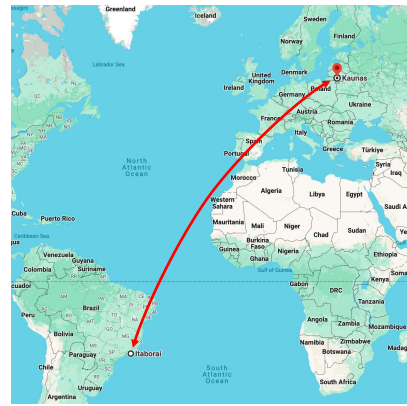
As shown in Fig. 10(a), the ground stations used in the experiment are located in Itaboraí (Brazil) and Kaunas (Lithuania). The straight-line distance between the two ground stations is approximately 10,000km.

1) *Ping*: Fig. 10(b) shows the ping value during the 1000s simulation under different algorithms. The ping values of LRST-1, LRST-2, and CSGI are all high, all around 500ms, and they are unstable. The ping value of C-LRST is relatively low, mostly staying around 160ms, with only a few jitters.

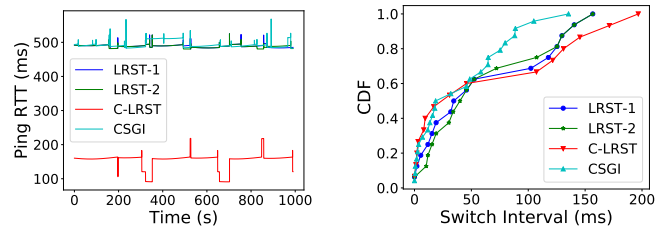
Based on the previously mentioned idea of classifying visible satellites, we can explain the ping values of the above algorithms: the ping value of LRST-1 is much higher than that of the other algorithms. This is because the access satellites selected by the two ground stations are located in two far-together categories. For the CSGI algorithm, although the path length is optimized from a global perspective, it is limited to connecting only one satellite and faces the same problems as LRST-1. Although LRST-2 maintains two GSLs, the ping value has almost no improvement compared with LRST-1. This is because the two satellites selected by each ground station during this period are in the same category, and the two categories are far apart. The C-LRST we proposed further classifies visible satellites on the basis of maintaining two GSLs, effectively avoiding the above-mentioned problems, and therefore has better performance.

2) *GSL switching interval*: Fig. 10(c) shows the time interval between each switching of the ground station's access satellite in a 1000s simulation. As long as the access satellite of either of the two ground stations changes, it is considered a switching. The switching of access satellite is the main cause of ping jitter.

As can be seen from Fig. 10(c), for LRST-1 and LRST-2, 14 switchings occur in the entire simulation process, C-LRST is 15, while CSGI is the most, up to 23. In addition, LRST-1, LRST-2, and C-LRST are at the lower right, which indicates that there is a longer time interval between two switchings, and the overall switching frequency is relatively low, making full use of the GSL that can be used for a longer time. The CSGI curve is near the upper left, the switching interval is short, and the switching frequency is slightly higher. Fig. 10(c) further



(a) Ground station pair from Itaboraí (Brazil) to Kaunas (Lithuania).



(b) Ping RTT. Compared to other algorithms, C-LRST has a lower Ping RTT. The fluctuations are due to the larger switching intervals and lower switching frequency.

Fig. 10. Ground station pair, Ping RTT, and GSL switching interval.

explains that in Fig. 10(b), CSGI has more ping jitters.

For CSGI, due to the limitation of connecting to only one satellite, even if it considers the overall situation, it cannot optimize the service duration and reduce the switching frequency for all ground stations. For example, in the experiment on the node pairs we selected above, the algorithm did not perform well. The C-LRST algorithm we proposed contains the idea of the longest remaining service time, retaining the advantage of lower switching frequency.

3) *Throughput*: Fig. 11 shows the throughput changes at the sender for different algorithms. The throughputs of the three algorithms LRST-1, LRST-2, and CSGI are low and unstable. For the C-LRST algorithm, the throughput can be stabilized at approximately 10Mbit/s relatively quickly, jittering occurs only at a few moments, and quickly recovers to 10Mbit/s.

One reason for low throughput is long delay. First, the slow start time is delayed due to the longer RTT. Second, a longer RTT means a longer congestion control period. For example, congestion that occurs at the receiving end takes a longer time to be perceived by the sending end, which makes congestion be processed more slowly and has a greater impact on throughput. In addition, due to the expansion of the scope of congestion, TCP Hybla will have fewer opportunities for fast retransmission and will instead enter a longer congestion avoidance state [46].

Another reason for low throughput is the high frequencies of link switching. As Fig. 11 shows, although CSGI imposes constraints on the minimum service time of access satellites, it

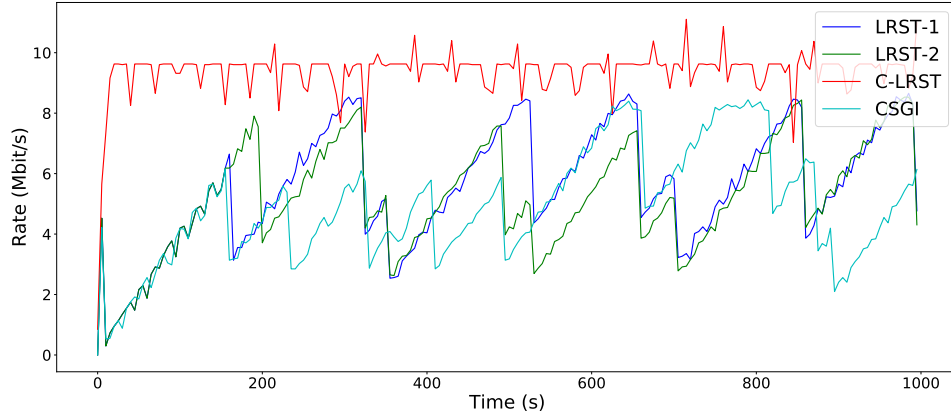


Fig. 11. Rate and Throughput. Over the entire simulation time, C-LRST has significantly stable and higher rate than other algorithms, which means that C-LRST has better throughput performance. The low rate of CSGI and other algorithms is due to the inefficient congestion handling caused by long latency, and the high GSL switching frequency.

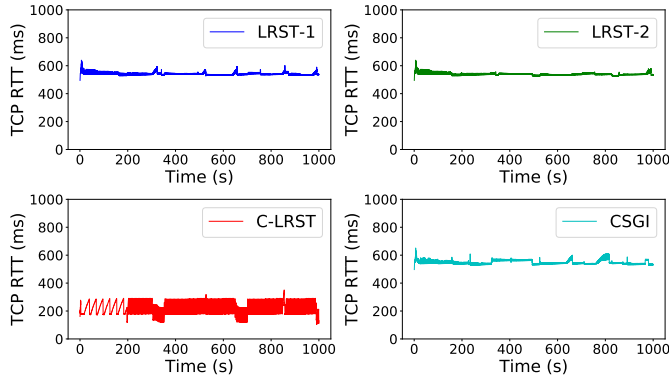


Fig. 12. TCP RTT. Compared to Ping RTT, TCP RTT also includes additional time such as packet processing, so it is slightly higher. However, the overall variation is consistent, and C-LRST has a lower RTT. The fluctuations are due to the characteristics of the TCP Hybla congestion control algorithm and have only a negligible effect.

is still unavoidable that multiple handovers occur in a short period. For example, around 160s and 660s, multiple switchings bring about a sharp decrease in throughput. At 405s, because the access satellites of two terminals are switched from (792, 56) to (827, 73), the ISL increases by 14 hops, which also causes a sharp decrease in throughput.

4) *TCP RTT*: Fig. 12 shows the performance of the TCP RTT using TCP Hybla congestion control algorithm. The results show that, C-LRST performs better, with an average value of approximately 250ms, while the values of CSGI, LRST-1, and LRST-2 are more than 500ms. The reason for the observed RTT results of TCP is consistent with the aforementioned Ping.

Then, we select 35 pairs of ground stations with different distances and perform end-to-end path analysis to provide a more comprehensive understanding of the four algorithms and make our findings more robust.

As shown in Fig. 13, the scattered points represent the average RTT of pairs with different distances under the corresponding algorithm, and the straight line is the linear fit of the scattered points. The overall RTT gradually increases with

the increasing distance, and some anomalies are due to the different switching numbers of different paths. From the linear fit, it can be seen that C-LRST has the lowest RTT in general, LRST-1 and LRST-2 are higher, and CSGI is the highest.

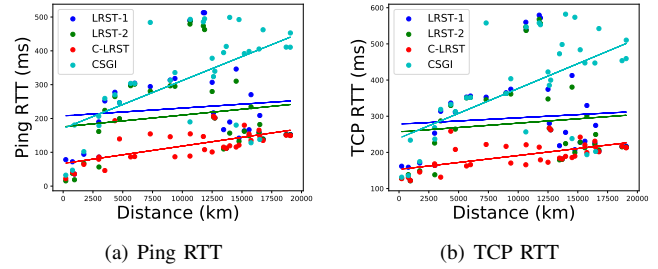


Fig. 13. Average RTT over distance between ground station pairs. Overall, C-LRST has the lowest average RTT, while CSGI has the highest.

D. Scalability

In order to study the scalability of the proposed C-LRST algorithm, we conduct experiments under a larger-scale constellation. Based on the basic scale, we double the number of orbits, thereby obtaining a constellation with twice the number of satellites.

We compare the communication performance of station pairs with different distances in the basic scale and the large scale constellations. As shown in Fig. 14, the scattered points represent the average RTT of ground station pairs during 1000s communication simulation, and the two straight lines are the linear fits of the scattered points.

The values of Ping RTT and TCP RTT of the two scale constellations are similar, which is expected. Even if the constellation scale is expanded, the communication links between the two nodes are similar, and thus there will be similar performance. However, with an increase in the number of satellites, a larger constellation may result in additional GSL switchings. Therefore, through linear fitting, it can be seen that in long-distance scenarios, the two values of the large scale

constellation have a slightly increasing trend, which is also in line with expectations.

Through comparative experiments, it can be seen that our C-LRST algorithm still has good adaptability in larger-scale constellation, and controls the more GSL switchings problem caused by the expansion of the constellation scale as much as possible, and has certain scalability.

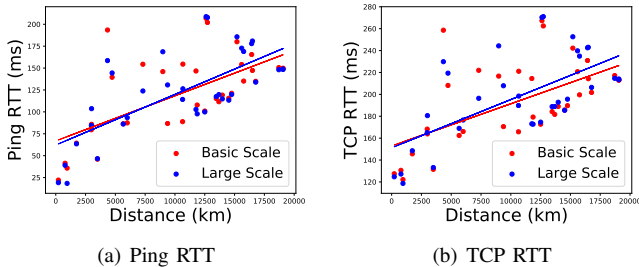


Fig. 14. Average RTT of C-LRST over distance between ground station pairs under two scale constellations. Compared with the basic scale, C-LRST still maintains good performance under a larger-scale constellation.

### E. Overhead and deployment

The computational complexity of the LRST algorithm depends on the operational complexity of calculating the longest service time satellites, so it is  $O(n)$ , where  $n$  is the number of visible satellites from the ground terminal. Since the classification is based on the flight direction of the satellite, this information can be directly obtained from the TLE data, so the complexity is  $O(n)$ . Although the complexity of CSGI is low during handover, the computational complexity is exponential when initializing the satellite connected to the ground station at the initial moment. In actual deployment, CSGI needs to grasp the information of all ground stations for coordinated scheduling, which is difficult to deploy in a scenario with a large number of ground stations. However, the satellite selection strategy of our algorithm is for each individual ground station, it only needs to know the satellite that can provide the longest remaining service time. The hardware conditions of each ground station can bear such a computing load. In addition, the design of our algorithm is based on an investigation of the existing infrastructure. As mentioned in the Introduction, the existing ground stations, such as Starlink, can provide multi-access capabilities. Therefore, our algorithm has good compatibility with existing infrastructure.

It should be pointed out that in the scenario of a larger number of satellites, there are more visible satellites on the ground station, and the calculation method of C-LRST will still generate certain costs. However, we would like to explain that this consideration of cost is limited to our experimental environment, and the calculation of visible satellite service time is essentially because the ground station needs to know the satellites information. However, in actual scenarios, the position, status, and other information of the satellites in the constellation will be monitored and fed back in real time. The ground station will easily know the satellite with the longest service time, and it will be easy to predict the satellite with the longest service time in the next moment

owing to the regularity of the satellite movement. Therefore, considering the differences between the actual scenario and the experimental environment, the overhead and efficiency of the actual deployment could be acceptable, even in a scenario with a large number of ground stations or satellites.

Unlike real-world network systems, there are natural bottlenecks in our experiments and performance evaluations due to the limited experimental conditions and simulation capabilities. However, our research is mainly aimed at contributing a design scheme for satellite-ground interconnection and providing a reference for future constellation construction. The application in a real scenario needs to consider various practical factors for corresponding adjustment and improvement.

## VI. CONCLUSION

In this paper, we propose the Classification-based Longest Remaining Service Time (C-LRST) algorithm. C-LRST supports the actual scenario with multi-access capabilities for terminals, and based on this, it adds more optional paths during routing with low computational complexity. In addition, we conduct experiments to evaluate our algorithm on the open-source constellation simulation platform Hypatia. We make adaptive improvements to the Hypatia platform to support our algorithm. Experiment results show that compared with current algorithms, the network delay of C-LRST is reduced by about 60%, the average throughput is increased by about 40%, and the link is more stable. Considering the access capabilities of current ground terminals, our algorithm is more suitable for application scenarios. As a potential future direction, we are looking forward to extending our C-LRST to improve the performance of various applications such as distributed learning systems [47], [48], [49], [50], [51], large language models [52], [53], [54], mobile edge computing [55], [56], [57], [58], [59], [60], [61], [62] etc in LEO satellite networks.

## REFERENCES

- [1] Y. Lei, G. Jianming *et al.*, "Leo mega-constellation network: Networking technologies and state of the art," *Journal on Communications*, vol. 43, no. 5, pp. 177–189, 2022.
- [2] Z. Lin, Z. Chen, Z. Fang, X. Chen, X. Wang, and Y. Gao, "Fedsn: A federated learning framework over heterogeneous leo satellite networks," *IEEE Transactions on Mobile Computing*, 2024.
- [3] Y. Zhang, Z. Lin, Z. Chen, Z. Fang, W. Zhu, X. Chen, J. Zhao, and Y. Gao, "Safed: A resource-efficient leo satellite-assisted heterogeneous federated learning framework," *arXiv preprint arXiv:2409.13503*, 2024.
- [4] H. Yuan, Z. Chen, Z. Lin, J. Peng, Z. Fang, Y. Zhong, Z. Song, and Y. Gao, "Satsense: Multi-satellite collaborative framework for spectrum sensing," *arXiv preprint arXiv:2405.15542*, 2024.
- [5] M. Giordani and M. Zorzi, "Non-terrestrial networks in the 6g era: Challenges and opportunities," *IEEE Network*, vol. 35, no. 2, pp. 244–251, 2021.
- [6] Z. Zhao, Z. Chen, Z. Lin, W. Zhu, K. Qiu, C. You, and Y. Gao, "Leo satellite networks assisted geo-distributed data processing," *arXiv preprint arXiv:2406.10856*, 2024.
- [7] H. Yuan, Z. Chen, Z. Lin, J. Peng, Z. Fang, Y. Zhong, Z. Song, X. Wang, and Y. Gao, "Graph learning for multi-satellite based spectrum sensing," in *2023 IEEE 23rd International Conference on Communication Technology (ICCT)*, 2023, pp. 1112–1116.
- [8] J. C. McDowell, "The low earth orbit satellite population and impacts of the spacex starlink constellation," *The Astrophysical Journal Letters*, vol. 892, no. 2, p. L36, 2020.
- [9] G. Curzi, D. Modenini, and P. Tortora, "Large constellations of small satellites: A survey of near future challenges and missions," *Aerospace*, vol. 7, no. 9, p. 133, 2020.

- [10] S. Ji, D. Zhou, M. Sheng, and J. Li, "Mega Satellite Constellation System Optimization: From a Network Control Structure Perspective," *IEEE Transactions on Wireless Communications*, vol. 21, no. 2, pp. 913–927, Feb. 2022, conference Name: IEEE Transactions on Wireless Communications.
- [11] Z. Lai, W. Liu, Q. Wu, H. Li, J. Xu, and J. Wu, "SpaceRTC: Unleashing the Low-latency Potential of Mega-constellations for Real-Time Communications," in *IEEE INFOCOM 2022 - IEEE Conference on Computer Communications*, May 2022, pp. 1339–1348, iSSN: 2641-9874.
- [12] Z. Luo, T. Pan, E. Song, H. Wang, W. Xue, T. Huang, and Y. Liu, "A Refined Dijkstra's Algorithm with Stable Route Generation for Topology-Varying Satellite Networks," in *2021 IEEE 41st International Conference on Distributed Computing Systems (ICDCS)*, Jul. 2021, pp. 1146–1147, iSSN: 2575-8411.
- [13] Z. Kassas, M. Neinavaie, J. Khalife, N. Khairallah, S. Kozhaya, J. Haidar-Ahmad, and Z. Shadram, "Enter leo on the gnss stage: Navigation with starlink satellites," 2021.
- [14] J. Wang, L. Li, and M. Zhou, "Topological dynamics characterization for leo satellite networks," *Computer Networks*, vol. 51, no. 1, pp. 43–53, 2007.
- [15] B. Al Homssi, A. Al-Hourani, K. Wang, P. Conder, S. Kandeepan, J. Choi, B. Allen, and B. Moores, "Next Generation Mega Satellite Networks for Access Equality: Opportunities, Challenges, and Performance," *IEEE Communications Magazine*, vol. 60, no. 4, pp. 18–24, Apr. 2022, conference Name: IEEE Communications Magazine.
- [16] E. Ekici, I. Akyildiz, and M. Bender, "A distributed routing algorithm for datagram traffic in LEO satellite networks," *IEEE/ACM Transactions on Networking*, vol. 9, no. 2, pp. 137–147, Apr. 2001, conference Name: IEEE/ACM Transactions on Networking.
- [17] A. Guidotti, A. Vanelli-Coralli, T. Foggi, G. Colavolpe, M. Caus, J. Bas, S. Cioni, and A. Modenini, "Lte-based satellite communications in leo mega-constellations," *International Journal of Satellite Communications and Networking*, vol. 37, no. 4, pp. 316–330, 2019.
- [18] H. Guo, Q. Yang, H. Wang, Y. Hua, T. Song, R. Ma, and H. Guan, "Spacedml: Enabling distributed machine learning in space information networks," *IEEE Network*, vol. 35, no. 4, pp. 82–87, 2021.
- [19] C. Yang, J. Yuan, Y. Wu, Q. Sun, A. Zhou, S. Wang, and M. Xu, "Communication-efficient satellite-ground federated learning through progressive weight quantization," *IEEE Transactions on Mobile Computing*, pp. 1–14, 2024.
- [20] Y. Tang, Z. Chen, A. Li, T. Zheng, Z. Lin, J. Xu, P. Lv, Z. Sun, and Y. Gao, "Merit: Multimodal wearable vital sign waveform monitoring," *arXiv preprint arXiv:2410.00392*, 2024.
- [21] J. Sun, C. Wu, S. Mumtaz, J. Tao, M. Cao, M. Wang, and V. Frascolla, "An efficient privacy-aware split learning framework for satellite communications," *IEEE Journal on Selected Areas in Communications*, 2024.
- [22] Z. Chen, T. Zheng, and J. Luo, "Octopus: A practical and versatile wideband mimo sensing platform," in *Proceedings of the 27th Annual International Conference on Mobile Computing and Networking*, 2021, pp. 601–614.
- [23] Z. Lin, G. Zhu, Y. Deng, X. Chen, Y. Gao, K. Huang, and Y. Fang, "Efficient parallel split learning over resource-constrained wireless edge networks," *IEEE Transactions on Mobile Computing*, 2024.
- [24] Z. Lin, G. Qu, Q. Chen, X. Chen, Z. Chen, and K. Huang, "Pushing large language models to the 6g edge: Vision, challenges, and opportunities," *arXiv preprint arXiv:2309.16739*, 2023.
- [25] Z. Chen, T. Zheng, C. Cai, and J. Luo, "Movi-fi: Motion-robust vital signs waveform recovery via deep interpreted rf sensing," in *Proceedings of the 27th annual international conference on mobile computing and networking*, 2021, pp. 392–405.
- [26] Z. Lin, L. Wang, J. Ding, B. Tan, and S. Jin, "Channel power gain estimation for terahertz vehicle-to-infrastructure networks," *IEEE Communications Letters*, vol. 27, no. 1, pp. 155–159, 2022.
- [27] J. Peng, Z. Chen, Z. Lin, H. Yuan, Z. Fang, L. Bao, Z. Song, Y. Li, J. Ren, and Y. Gao, "Sums: Sniffing unknown multiband signals under low sampling rates," *arXiv preprint arXiv:2405.15705*, 2024.
- [28] X. Yang, J. Chen, K. He, H. Bai, C. Wu, and R. Du, "Efficient privacy-preserving inference outsourcing for convolutional neural networks," *IEEE Transactions on Information Forensics and Security*, vol. 18, pp. 4815–4829, 2023.
- [29] X. Cao and X. Zhang, "Satpc: Link-layer informed tcp adaptation for highly dynamic leo satellite networks," in *IEEE INFOCOM 2023 - IEEE Conference on Computer Communications*, 2023, pp. 1–10.
- [30] S. Ma, Y. C. Chou, H. Zhao, L. Chen, X. Ma, and J. Liu, "Network characteristics of leo satellite constellations: A starlink-based measurement from end users," in *IEEE INFOCOM 2023 - IEEE Conference on Computer Communications*, 2023, pp. 1–10.
- [31] Y. Zhang, Q. Wu, Z. Lai, and H. Li, "Enabling Low-latency-capable Satellite-Ground Topology for Emerging LEO Satellite Networks," in *IEEE INFOCOM 2022 - IEEE Conference on Computer Communications*, May 2022, pp. 1329–1338, iSSN: 2641-9874.
- [32] "Attachment Narrative SES-AMD-20200605-00606." [Online]. Available: <https://www.fcc.report/IBFS/SES-AMD-20200605-00606/2412055>
- [33] "Space-Track.org." [Online]. Available: <https://www.space-track.org/documentation/tle>
- [34] C.-J. Wang, "Structural properties of a low Earth orbit satellite constellation - the Walker delta network," in *Proceedings of MILCOM '93 - IEEE Military Communications Conference*, vol. 3, Oct. 1993, pp. 968–972 vol.3.
- [35] D. Bhattacharjee and A. Singla, "Network topology design at 27,000 km/hour," in *Proceedings of the 15th International Conference on Emerging Networking Experiments And Technologies*, 2019, pp. 341–354.
- [36] X. Xu, C. Wang, and Z. Jin, "An analysis method for isl of multilayer constellation," *Journal of Systems Engineering and Electronics*, vol. 33, no. 4, pp. 961–968, 2022.
- [37] A. U. Chaudhry and H. Yanikomeroğlu, "Laser intersatellite links in a starlink constellation: A classification and analysis," *IEEE Vehicular Technology Magazine*, vol. 16, no. 2, pp. 48–56, 2021.
- [38] S. Cakaj, B. Kamo, A. Lala, and A. Rakipi, "Elevation impact on signal to spectral noise density ratio for Low Earth Orbiting satellite ground station at S-band," in *2014 Science and Information Conference*, Aug. 2014, pp. 641–645.
- [39] H. Uzunalioglu, I. F. Akyildiz, Y. Yesha, and W. Yen, "Footprint handover rerouting protocol for low Earth orbit satellite networks," *Wireless Networks*, vol. 5, no. 5, pp. 327–337, Sep. 1999. [Online]. Available: <https://doi.org/10.1023/A:1019127801155>
- [40] Z. Lai, W. Liu, Q. Wu, H. Li, J. Xu, and J. Wu, "Spacertc: Unleashing the low-latency potential of mega-constellations for real-time communications," in *IEEE INFOCOM 2022 - IEEE Conference on Computer Communications*, 2022, pp. 1339–1348.
- [41] Q. Chen, G. Giambene, L. Yang, C. Fan, and X. Chen, "Analysis of inter-satellite link paths for leo mega-constellation networks," *IEEE Transactions on Vehicular Technology*, vol. 70, no. 3, pp. 2743–2755, 2021.
- [42] S. Kassing, D. Bhattacharjee, A. B. Águas, J. E. Saethre, and A. Singla, "Exploring the "Internet from space" with Hypatia," in *Proceedings of the ACM Internet Measurement Conference*, ser. IMC '20. New York, NY, USA: Association for Computing Machinery, Oct. 2020, pp. 214–229. [Online]. Available: <https://dl.acm.org/doi/10.1145/3419394.3423635>
- [43] starlink.sx. [Online]. Available: <https://starlink.sx/>
- [44] S. Liu, F. Xu *et al.*, "Starlink actual constellation configuration research and simulation analysis," *Space and Internet*, 10 2022. [Online]. Available: <https://mp.weixin.qq.com/s/nk49ZKewwFCiBQri5VzetA>
- [45] Lmcn-sgi. [Online]. Available: <https://github.com/jingjiuxiaoshishu/LMCN-SGI>
- [46] M. Casoni, C. A. Grazia, M. Klapez, and N. Patriciello, "Implementation and validation of TCP options and congestion control algorithms for ns-3," in *Proceedings of the 2015 Workshop on ns-3*, ser. WNS3 '15. New York, NY, USA: Association for Computing Machinery, May 2015, pp. 112–119. [Online]. Available: <https://dl.acm.org/doi/10.1145/2756509.2756518>
- [47] Z. Lin, G. Qu, X. Chen, and K. Huang, "Split learning in 6g edge networks," *IEEE Wireless Communications*, 2024.
- [48] J. Hu, Z. Chen, T. Zheng, R. Schober, and J. Luo, "Holofed: Environment-adaptive positioning via multi-band reconfigurable holographic surfaces and federated learning," *IEEE Journal on Selected Areas in Communications*, 2023.
- [49] T. Zheng, A. Li, Z. Chen, H. Wang, and J. Luo, "Autofed: Heterogeneity-aware federated multimodal learning for robust autonomous driving," in *Proceedings of the 29th Annual International Conference on Mobile Computing and Networking*, 2023, pp. 1–15.
- [50] M. Hu, J. Zhang, X. Wang, S. Liu, and Z. Lin, "Accelerating federated learning with model segmentation for edge networks," *IEEE Transactions on Green Communications and Networking*, 2024.
- [51] Z. Lin, G. Qu, W. Wei, X. Chen, and K. K. Leung, "Adaptsfl: Adaptive split federated learning in resource-constrained edge networks," *arXiv preprint arXiv:2403.13101*, 2024.
- [52] Z. Lin, X. Hu, Y. Zhang, Z. Chen, Z. Fang, X. Chen, A. Li, P. Vepakomma, and Y. Gao, "Splitlora: A split parameter-efficient

- fine-tuning framework for large language models,” *arXiv preprint arXiv:2407.00952*, 2024.
- [53] Z. Fang, Z. Lin, Z. Chen, X. Chen, Y. Gao, and Y. Fang, “Automated federated pipeline for parameter-efficient fine-tuning of large language models,” *arXiv preprint arXiv:2404.06448*, 2024.
- [54] Y. Qiu, H. Chen, X. Dong, Z. Lin, I. Y. Liao, M. Tistarelli, and Z. Jin, “Ifvit: Interpretable fixed-length representation for fingerprint matching via vision transformer,” *arXiv preprint arXiv:2404.08237*, 2024.
- [55] Y. Gu, J. Chen, C. Wu, K. He, Z. Zhao, and R. Du, “Loccams: An efficient and robust approach for detecting and localizing hidden wireless cameras via commodity devices,” *Proceedings of the ACM on Interactive, Mobile, Wearable and Ubiquitous Technologies*, vol. 7, no. 4, pp. 1–24, 2024.
- [56] Z. Lin, L. Wang, J. Ding, Y. Xu, and B. Tan, “Tracking and transmission design in terahertz v2i networks,” *IEEE Transactions on Wireless Communications*, vol. 22, no. 6, pp. 3586–3598, 2022.
- [57] T. Zheng, Z. Chen, S. Zhang, C. Cai, and J. Luo, “More-fi: Motion-robust and fine-grained respiration monitoring via deep-learning uwb radar,” in *Proceedings of the 19th ACM conference on embedded networked sensor systems*, 2021, pp. 111–124.
- [58] Z. Lin, L. Wang, J. Ding, Y. Xu, and B. Tan, “V2i-aided tracking design,” in *ICC 2022-IEEE International Conference on Communications*. IEEE, 2022, pp. 291–296.
- [59] Z. Chen, C. Cai, T. Zheng, J. Luo, J. Xiong, and X. Wang, “Rf-based human activity recognition using signal adapted convolutional neural network,” *IEEE Transactions on Mobile Computing*, vol. 22, no. 1, pp. 487–499, 2021.
- [60] Z. Fang, Z. Lin, S. Hu, H. Cao, Y. Deng, X. Chen, and Y. Fang, “Ic3m: In-car multimodal multi-object monitoring for abnormal status of both driver and passengers,” *arXiv preprint arXiv:2410.02592*, 2024.
- [61] C. Wu, H. Cao, G. Xu, C. Zhou, J. Sun, R. Yan, Y. Liu, and H. Jiang, “It’s all in the touch: Authenticating users with host gestures on multi-touch screen devices,” *IEEE Transactions on Mobile Computing*, 2024.
- [62] C. Wu, J. Chen, Q. Fang, K. He, Z. Zhao, H. Ren, G. Xu, Y. Liu, and Y. Xiang, “Rethinking membership inference attacks against transfer learning,” *IEEE Transactions on Information Forensics and Security*, 2024.